Title	Mechanism of low-temperature-annealed Ohmic contacts to AlGaN/GaN heterostructures: A study via formation and removal of Ta-based Ohmic-metals
Author(s)	Uryu, Kazuya; Kiuchi, Shota; Sato, Taku; Suzuki, Toshi-kazu
Citation	Applied Physics Letters, 120(5): 052104
Issue Date	2022-02-03
Type	Journal Article
Text version	publisher
URL	http://hdl.handle.net/10119/19954
Rights	Copyright (c) 2022 AIP Publishing. This article may be downloaded for personal use only. Any other use requires prior permission of the author and AIP Publishing. This article appeared in Kazuya Uryu, Shota Kiuchi, Taku Sato, Toshi-kazu Suzuki; Mechanism of low-temperature-annealed Ohmic contacts to AlGaN/GaN heterostructures: A study via formation and removal of Ta-based Ohmic-metals, Applied Physics Letters, 3 February 2022; 120 (5): 052104 and may be found at https://doi.org/10.1063/5.0080265.
Description	

Mechanism of low-temperature-annealed Ohmic contacts to AlGaN/GaN heterostructures: A study via formation and removal of Ta-based Ohmic-metals ⊘

Kazuya Uryu; Shota Kiuchi; Taku Sato; Toshi-kazu Suzuki ✉ ⓘ

Check for updates

View Online   Export Citation

Articles You May Be Interested In

Electrical characterization of AlGaN/GaN heterostructures under Ohmic metals by using multi-probe Hall devices
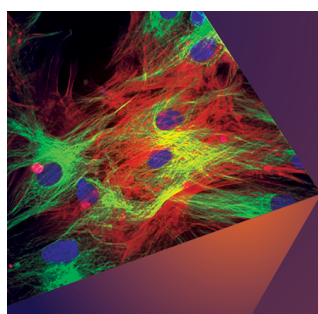
Appl. Phys. Lett. (July 2021)

Low-temperature-annealed Ohmic contacts to ultrathin-AlGaN/GaN heterostructures with no two-dimensional electron gas

Appl. Phys. Lett. (June 2025)

Sheet resistance under Ohmic contacts to AlGaN/GaN heterostructures

Appl. Phys. Lett. (June 2014)

Mechanism of low-temperature-annealed Ohmic contacts to AlGaN/GaN heterostructures: A study via formation and removal of Ta-based Ohmic-metals

Kazuya Uryu,[1,2] Shota Kiuchi,[1] Taku Sato,[2] and Toshi-kazu Suzuki[1,a] (iD)

AFFILIATIONS

[1]Center for Nano Materials and Technology, Japan Advanced Institute of Science and Technology (JAIST), 1-1 Asahidai, Nomi, Ishikawa 923-1292, Japan

[2]Advantest Laboratories Ltd., 48-2 Matsubara, Kami-Ayashi, Aoba-ku, Sendai, Miyagi 989-3124, Japan

[a]Author to whom correspondence should be addressed: tosikazu@jaist.ac.jp

ABSTRACT

We studied the mechanism of low-temperature-annealed Ohmic contacts to AlGaN/GaN heterostructures via formation and removal of Ta/Al/Ta Ohmic-metals. Multi-probe Hall device measurements show one order increase in the sheet electron concentration after Ohmic-metal formation compared with that before formation, indicating that high-density doping takes place in the AlGaN/GaN heterostructure under the Ohmic-metal. However, after Ohmic-metal removal, the increased sheet electron concentration returns to the value before formation. Moreover, we formed Ni/Au Schottky contacts on the AlGaN/GaN heterostructures before Ohmic-metal formation and after Ohmic-metal removal, and confirmed that the characteristics are almost the same. These results indicate that donors do not exist after Ohmic-metal removal, suggesting that, although high-density doping takes place, high-density donors are not formed under the Ohmic-metal. The high-density doping *without* high-density donors could be attributed to polarization doping, playing a significant role in Ohmic contact formation.

Published under an exclusive license by AIP Publishing. https://doi.org/10.1063/5.0080265

To date, there have been many attempts to obtain good Ohmic contacts for wide-gap GaN-based devices.[1] In particular, Ohmic-metal structures for AlGaN/GaN heterostructures have been extensively investigated, where an Ohmic contact is obtained by an electrical coupling between the surface Ohmic-metal and the underlying two dimensional electron gas (2DEG) through the AlGaN energy barrier. In early studies, Ohmic contacts for AlGaN/GaN heterostructures are obtained by high-temperature annealing at $\gtrsim 800\,^\circ$C for Ti-based[2–7] and Ta-based[8–11] multilayer structures. However, in order to reduce the thermal budget, and to suppress rough surface morphology and poor edge acuity of Ohmic-metals,[12] lower-temperature annealing is preferable. Recently, Ohmic contacts are obtained by low-temperature annealing at 500–600 °C.[13–19] Table I summarizes Ohmic contact resistances R_c to AlGaN/GaN heterostructures, which are obtained by high-temperature or low-temperature annealing for Ti-based or Ta-based multilayer structures. This indicates that low R_c can be obtained even by low-temperature annealing, being useful for low on-resistance

devices. For example, normally-off AlGaN/GaN MOSFETs with low on-resistance $\sim 4\ \Omega$ mm were realized,[20] where a $R_c \sim 0.3\ \Omega$ mm Ta-based Ohmic contact annealed at 550 °C was employed.

As a formation mechanism of low-temperature-annealed Ohmic contacts, metallic material penetration into the AlGaN/GaN heterostructures, which is observed for high-temperature annealing[3,21] with metallic temperature dependence of the contact resistance,[21] is not probable. In fact, for low-temperature annealing, scanning transmission electron microscope (STEM) observations indicate no metallic material penetration,[15–18] and temperature dependence of the contact resistance is not metallic.[18] Thus, as a plausible mechanism, donor doping by nitrogen vacancies in the AlGaN layer is assumed,[15,17,18] associated with a nanometer-order thick metallic nitride layer between the AlGaN layer and the Ohmic-metal. However, since the nanometer-order thick metallic nitride layer requires generation of nitrogen vacancies $\sim 10^{20}$ cm^{-3} over a micrometer-order thick AlGaN/GaN layer, it was pointed out that

27 June 2025 03:27:42

TABLE I. Summary of Ohmic contact resistances R_c to AlGaN/GaN heterostructures, obtained by high-temperature (HT) or low-temperature (LT) annealing for Ti-based or Ta-based multilayer structures.

	Ti-based	Ta-based
HT (800–950 °C)	0.12–1.2 Ω mm (Refs. 2–7)	0.20–0.24 Ω mm (Refs. 8–11)
LT (500–600 °C)	0.21–0.65 Ω mm (Refs. 13 and 14)	0.24–0.80 Ω mm (Refs. 15–18)

generation of nitrogen vacancies is quantitatively questionable.[7] Moreover, it is difficult to directly observe nitrogen vacancies in nitride materials; there is no direct observation of the nitrogen vacancies.

When doping takes place in a semiconductor under an Ohmic-metal, the electrical properties are modified from those before Ohmic-metal formation. In order to measure the modified electrical properties, the end contact resistance method[12,22–31] and the floating contact resistance method[32–34] have been developed. However, these methods can measure only the sheet resistance ρ_s; the carrier concentration and the carrier mobility cannot be evaluated. Recently, by using multi-probe Hall devices, we developed a method to characterize the carrier concentration and the carrier mobility under an Ohmic-metal.[35] Applying the method, we observed significant increases in the sheet electron concentration n_s of AlGaN/GaN heterostructures under low-temperature-annealed Ti-based Ohmic-metals, indicating that high-density doping takes place under the Ohmic-metals. In addition, we found that the electron mobility μ_s is too high for ionized impurity scattering,[36] assuming donor doping by nitrogen vacancies or diffused metal atoms. We consider that polarization doping due to a strain induced by the Ohmic-metals has a contribution to the high-density doping, because polarization doping is not associated with ionized donor scattering, giving high μ_s even for high-density doping.[37–39]
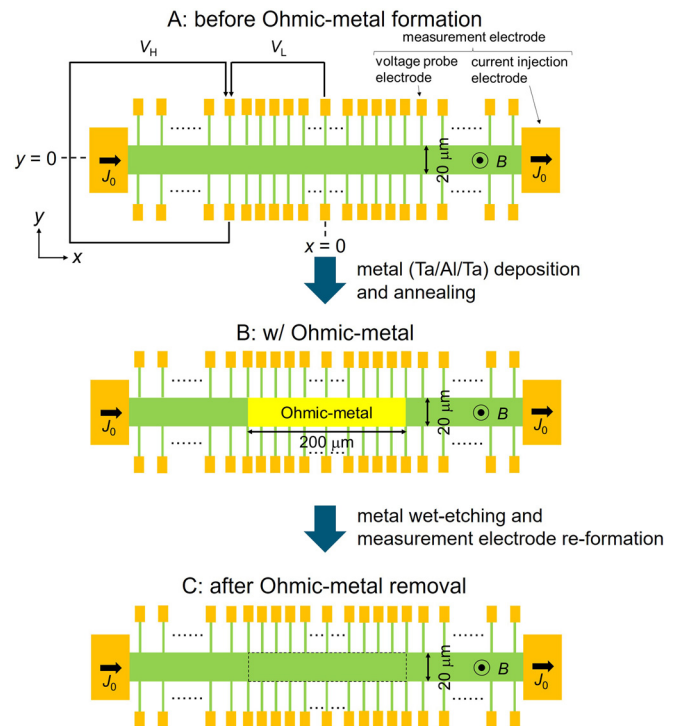
If high-density donors exist under an Ohmic-metal, we can expect that the electrical properties even after Ohmic-metal removal will be different from those before formation. In this work, we studied the mechanism of low-temperature-annealed Ohmic contacts to AlGaN/GaN heterostructures via formation and removal of Ta/Al/Ta Ohmic-metals. By using multi-probe Hall devices, we characterized electrical properties of AlGaN/GaN heterostructures before and after Ohmic-metal formation, and also after Ohmic-metal removal. Moreover, we formed and investigated Ni/Au Schottky contacts on the AlGaN/GaN heterostructures before Ohmic-metal formation and after Ohmic-metal removal.

We fabricated multi-probe Hall devices (Samples A, B, and C) shown in Fig. 1, using an undoped-$Al_{0.24}Ga_{0.76}N$(20 nm)/GaN(3000 nm) heterostructure grown by metal-organic chemical vapor deposition on sapphire (0001). In order to define the channel regions, device isolation was achieved by B^+ ion implantation. According to the *x-y* coordinates shown in Fig. 1 with the origin at the center of the channel, the channel region is $-320 \leq x \leq +320\,\mu m$ and $-10 \leq y \leq +10\,\mu m$. The devices have measurement electrodes consisting of current injection and voltage probe electrodes. Sample A is the device before Ohmic-metal formation. Sample B is the device with a Ta/Al/Ta Ohmic-metal of length $L = 200\,\mu m$ ($-100 \leq x \leq +100\,\mu m$) and width $W = 20\,\mu m$ ($-10 \leq y \leq +10\,\mu m$), formed by annealing at 575 °C giving $R_c \simeq 0.45\,\Omega$ mm. Sample C is the device after Ohmic-metal removal, where the metal and the measurement electrodes were wet-etched by $H_2O_2 : H_2SO_4$ (1:9) and HF, and subsequently, the

measurement electrodes were re-formed. As defined in Fig. 1, we measured the voltage drop V_L under no magnetic field $B = 0$ and V_H under magnetic field $B = 0.32$ T as a function of the position x, applying measurement current densities $-45 \leq J_0 \leq +45$ mA/mm through the current injection electrodes.

Figure 2 shows the measured $V_L(x)/J_0$ and $V_H(x)/J_0$ for Samples A and B. For Sample A, a linear behavior for $V_L(x)/J_0$ and a constant behavior for $V_H(x)/J_0$ are observed, giving $\rho_s \simeq 530\,\Omega/\square$, $n_s \simeq 0.73 \times 10^{13}$ cm^{-2}, and $\mu_s \simeq 1600$ cm^2/V-s. On the other hand, for Sample B, $V_L(x)/J_0$ shows a nonlinear behavior and $V_H(x)/J_0$ is not constant. In the Ohmic-metal region, the nonlinear behavior can be analyzed by using the method reported in Ref. 35, where a transmission line model gives

$$\frac{V_L(x)}{J_0} = -\frac{\rho_s}{\rho_s + \rho_m}$$
$$\times \left(\rho_m x + \rho_s \frac{\sinh(\sqrt{(\rho_s + \rho_m)/\rho_c}\,x)}{\sqrt{(\rho_s + \rho_m)/\rho_c}\cosh(\sqrt{(\rho_s + \rho_m)/\rho_c}L/2)} \right),$$

(1)

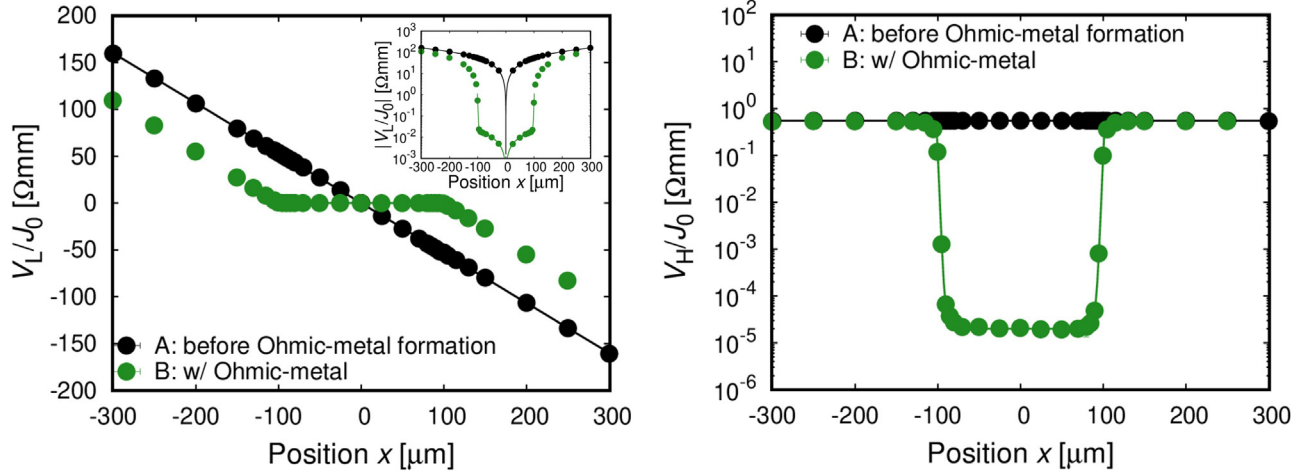**FIG. 1.** The schematic top view of multi-probe Hall devices.

FIG. 2. The measured $V_L(x)/J_0$ (left) and $V_H(x)/J_0$ (right) with the fitting curves for Samples A and B. The inset of the left figure: the measured $V_L(x)/J_0$ in a logarithmic scale for Samples A and B.

using the metal sheet resistance ρ_m and specific contact resistivity ρ_c, and

$$\frac{V_H(0)}{j_s(0)BW} \simeq \mu_s \rho_s = \frac{1}{qn_s}, \qquad (2)$$

with $j_s(x) = -V_L'(x)/\rho_s$ and the electron charge q. As shown in Fig. 2, we can obtain good fitting for $V_L(x)/J_0$ using (1), leading to $\rho_s \simeq (400 \pm 50)\ \Omega/\square$ and $\rho_c \simeq (4.9 \pm 0.7) \times 10^{-6}\ \Omega\,cm^2$. We also obtain $n_s \simeq (9.3 \pm 1.2) \times 10^{13}\ cm^{-2}$ and $\mu_s \simeq (170 \pm 10)\ cm^2/V\text{-}s$ using (2). This indicates that n_s significantly increases by Ohmic-metal formation. In addition, the $n_s \simeq 9.3 \times 10^{13}\ cm^{-2}$ after formation is much larger than the maximum value in the 2DEG channel $\sim 1.3 \times 10^{13}\ cm^{-2}$ without parallel conduction in the AlGaN/GaN heterostructures; above this value, conduction electrons exist in the AlGaN layer. This suggests that parallel conduction occurs in the

20 nm-thickness AlGaN layer with a sheet electron concentration of $\sim 8.0 \times 10^{13}\ cm^{-2}$, and thus, the doping concentration N_D in the AlGaN layer is $\gtrsim 4 \times 10^{19}\ cm^{-3}$.

In order to confirm N_D in the AlGaN/GaN heterostructure under the Ohmic-metal, we characterized the temperature dependence of ρ_c obtained from $V_L(x)/J_0$ measurements. Figure 3 shows the measured $V_L(x)/J_0$ for the temperature $T = 250\text{–}320\ K$ with curves fitted by using (1), giving ρ_c as a function of T shown in Fig. 4. The result in Fig. 4 can be fitted by the field emission (FE) model,[40] as expected since the $N_D \gtrsim 4 \times 10^{19}\ cm^{-3}$ satisfies the following criterion for the dominance of the FE:[41,42] $k_B T < 2E_{00}/[\ln(4\Phi_B/E_F) + (2E_{00}/E_F)^{1/2}]$, where k_B is the Boltzmann constant, $E_{00} = q\hbar\sqrt{N_D/m^*\varepsilon_s}/2$, $\hbar$ is the Dirac constant, m^* is the semiconductor electron effective mass, ε_s is the semiconductor dielectric constant, Φ_B is the barrier height,
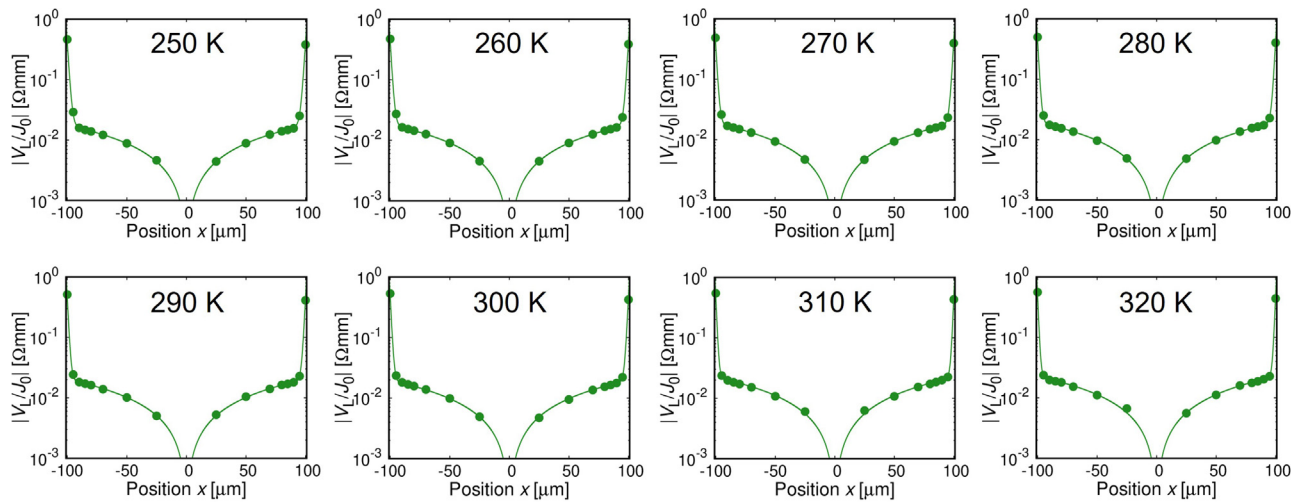
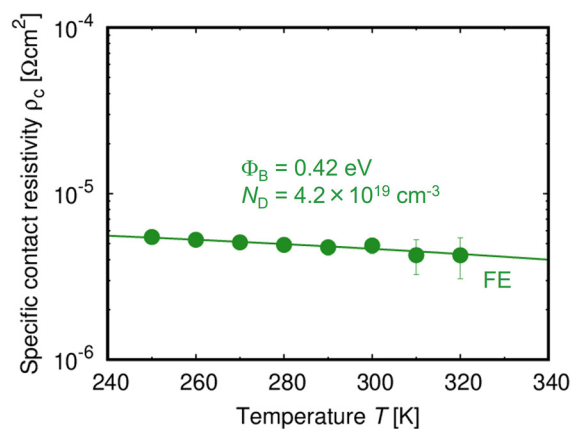FIG. 3. The measured $V_L(x)/J_0$ as a function of the position with the fitting curves at 250–320 K for Sample B.

FIG. 4. The specific contact resistivity ρ_c as a function of the temperature T with the fitting curve for Sample B.
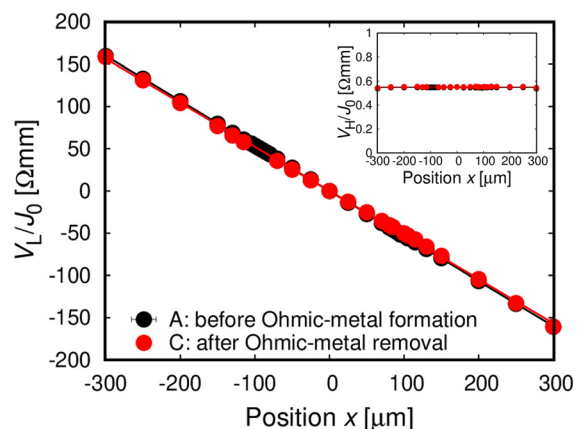

FIG. 6. The measured $V_L(x)/J_0$ with the fitting curves for Samples A and C. The inset: the measured $V_H(x)/J_0$ with the fitting curves for Samples A and C.
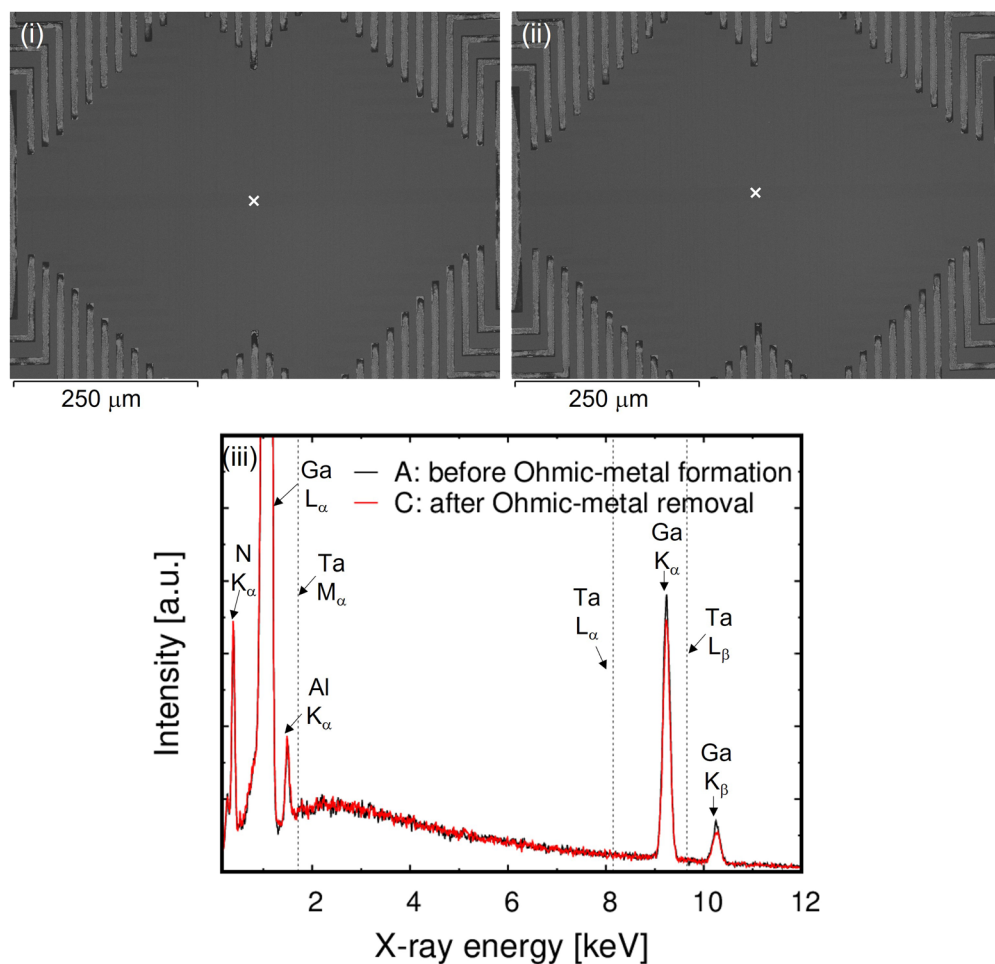

FIG. 5. The SEM image for (i) Sample A and (ii) Sample C. (iii) The EDS spectra measured at the cross mark positions in (i) and (ii).

27 June 2025 03:27:42

TABLE II. Summary of the 2DEG properties and the surface roughnesses of Samples A and C.

Sample	ρ_s ($\Omega/\square$)	n_s (10^{13} cm^{-2})	μ_s (cm^2/V s)	RMS surface roughness (nm)
A: before Ohmic-metal formation	530	0.73	1600	0.5
C: after Ohmic-metal removal	520	0.72	1650	0.4

and E_F is the semiconductor Fermi energy. The fitting gives $N_D \simeq 4.2 \times 10^{19}$ cm^{-3} and $\Phi_B \simeq 0.42$ eV.

For Sample A, before Ohmic-metal formation, and Sample C, after Ohmic-metal removal, energy dispersive x-ray spectroscopy (EDS) was carried out in a scanning electron microscope (SEM) operated at 15 keV. The SEM images are shown in Fig. 5(i) for Sample A and in Fig. 5(ii) for Sample C. Figure 5(iii) shows the EDS spectra measured at the cross mark positions in Figs. 5(i) and 5(ii). These spectra almost coincide, and there is no peak of Ta, confirming that the Ohmic-metal is completely removed by wet-etching. In addition, atomic force microscopy (AFM) was carried out for the AlGaN surface
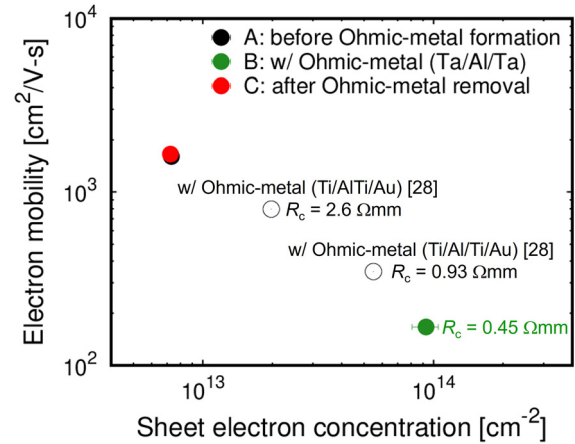
FIG. 7. The relation between the sheet electron concentration and the electron mobility for Samples A–C, where the values for Ti-based Ohmic contacts are simultaneously shown for comparison.

of Samples A and C, showing almost similar root mean square (RMS) surface roughnesses of $\simeq 0.5$ nm (Sample A) and $\simeq 0.4$ nm (Sample C). Figure 6 and the inset show the measured $V_L(x)/J_0$ and $V_H(x)/J_0$, respectively, for Samples A and C. The results for Sample C are almost
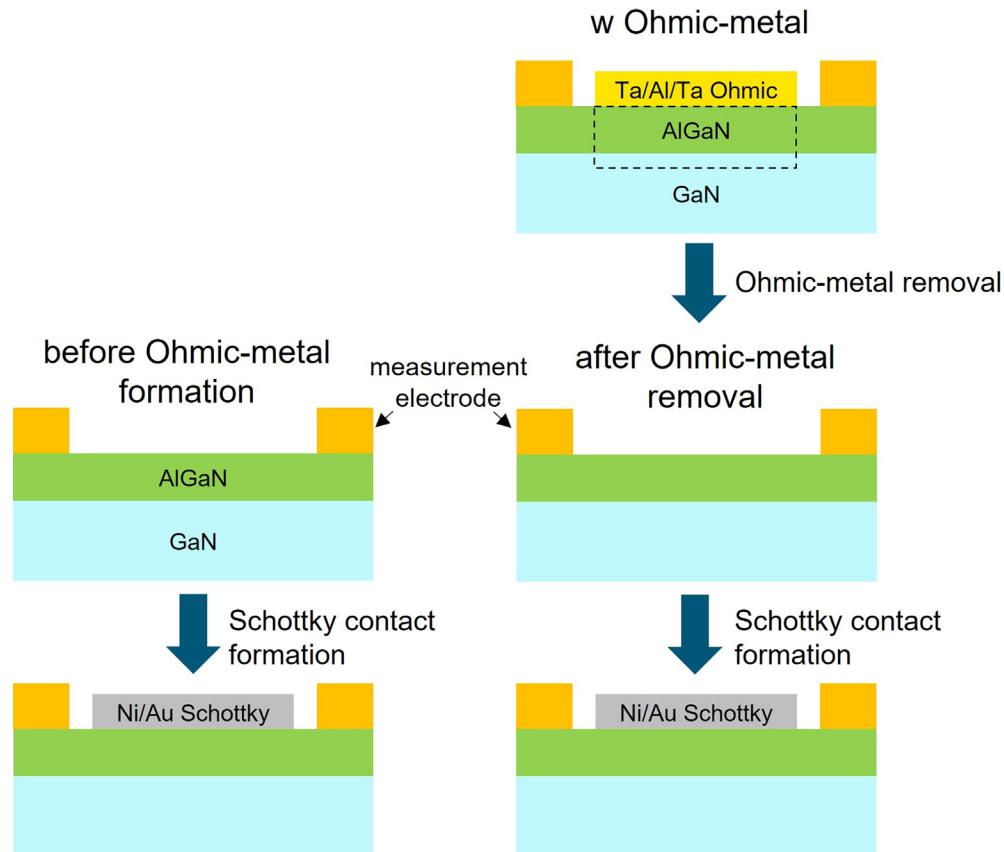
FIG. 8. The fabrication process of Ni/Au Schottky contacts on the AlGaN/GaN heterostructures before Ohmic-metal formation and after Ohmic-metal removal.

unchanged from those for Sample A, giving $\rho_s \simeq 520\ \Omega/\square$, $n_s \simeq 0.72 \times 10^{13}\ \mathrm{cm}^{-2}$, and $\mu_s \simeq 1650\ \mathrm{cm^2/V\text{-}s}$, as listed in Table II with the RMS surface roughnesses.

The obtained n_s and μ_s are summarized in Fig. 7, where the values for Ti-based Ohmic contacts[35] are simultaneously shown for comparison, showing that n_s increases with a decrease in the contact resistance R_c. After Ohmic-metal removal, the significantly increased n_s by Ohmic-metal formation returns to the value before formation. This indicates that high-density doping in the semiconductor under the Ohmic-metal dose not remain after Ohmic-metal removal.

In addition, we formed and electrically characterized Ni/Au Schottky contacts (a diameter of 80 μm) on the AlGaN/GaN heterostructures before Ohmic-metal formation and after Ohmic-metal removal, according to the process flow shown in Fig. 8. As shown in Fig. 9, we find that the capacitance-voltage characteristics for both Schottky contacts almost coincide even in the logarithmic scale, indicating that the dielectric property after Ohmic-metal removal is unchanged from that before Ohmic-metal formation. Moreover, as shown in the inset of Fig. 9, the current-voltage characteristics are almost similar. Both Schottky diodes have almost the same characteristics with barrier heights $\simeq 1.6$ eV, ideality factors $\simeq 1.3$–1.4, and series resistances $\sim 30\ \Omega$. Therefore, we can confirm that donors do not exist after Ohmic-metal removal; although high-density doping takes place, high-density donors are not formed under the Ohmic-metal. Since polarization doping is not associated with donors, we consider that the high-density doping without high-density donors is attributed to polarization doping due to the strain induced by the Ohmic-metal. This has a similarity to 2DEG concentration enhancements due to strains induced by passivation films for AlGaN/GaN heterostructures.[43]

In summary, we investigated formation and removal of the low-temperature-annealed Ta-based Ohmic-metals on the AlGaN/GaN heterostructures. We find one order increase in n_s after Ohmic-metal formation compared with that before formation, indicating that high-density doping takes place in the AlGaN/GaN heterostructure. However, after Ohmic-metal removal, n_s returns to the value before

Ohmic-metal formation. In addition, we find that the Ni/Au Schottky contacts on the AlGaN/GaN heterostructures before Ohmic-metal formation and after Ohmic-metal removal show the same characteristics. These results indicate that donors do not exist after Ohmic-metal removal, suggesting that, although high-density doping takes place, high-density donors are not formed under the Ohmic-metal. The high-density doping *without* high-density donors could be attributed to polarization doping, playing a significant role in Ohmic contact formation.

AUTHOR DECLARATIONS
Conflict of Interest

The authors have no conflicts to disclose.

DATA AVAILABILITY

The data that support the findings of this study are available from the corresponding author upon reasonable request.

REFERENCES

[1]G. Greco, F. Iucolano, and F. Roccaforte, Appl. Surf. Sci **383**, 324 (2016).
[2]Q. Z. Liu, L. S. Yu, F. Deng, S. S. Lau, Q. Chen, J. W. Yang, and M. A. Khan, Appl. Phys. Lett. **71**, 1658 (1997).
[3]L. Wang, F. M. Mohammed, and I. Adesida, J. Appl. Phys. **101**, 013702 (2007).
[4]H.-S. Lee, D. S. Lee, and T. Palacios, IEEE Electron Device Lett. **32**, 623 (2011).
[5]S. Arulkumaran, S. Vicknesh, N. G. Ing, S. L. Selvaraj, and T. Egawa, Appl. Phys. Express **4**, 084101 (2011).
[6]D. H. Zadeh, S. Tanabe, N. Watanabe, and H. Matsuzaki, Jpn. J. Appl. Phys., Part 1 **55**, 05FH06 (2016).
[7]A. Shriki, R. Winter, Y. Calahorra, Y. Kauffmann, G. Ankonina, M. Eizenberg, and D. Ritter, J. Appl. Phys. **121**, 065301 (2017).
[8]D. Qiao, L. Jia, L. S. Yu, P. M. Asbeck, S. S. Lau, S.-H. Lim, Z. Liliental-Weber, T. E. Haynes, and J. B. Barner, J. Appl. Phys. **89**, 5543 (2001).
[9]S. Arulkumaran, G. I. Ng, S. Vicknesh, H. Wang, K. S. Ang, C. M. Kumar, K. L. Teo, and K. Ranjan, Appl. Phys. Express **6**, 016501 (2013).
[10]Y. Li, G. I. Ng, S. Arulkumaran, C. M. M. Kumar, K. S. Ang, M. J. Anand, H. Wang, R. Hofstetter, and G. Ye, Appl. Phys. Express **6**, 116501 (2013).
[11]Y. Li, G. I. Ng, S. Arulkumaran, G. Ye, C. M. M. Kumar, M. J. Anand, and Z. H. Liu, Appl. Phys. Express **8**, 041001 (2015).
[12]Y. Sun, X. Chen, and L. F. Eastman, J. Appl. Phys. **98**, 053701 (2005).
[13]M. Van Hove, S. Boulay, S. R. Bahl, S. Stoffels, X. Kang, D. Wellekens, K. Geens, A. Delabie, and S. Decoutere, IEEE Electron Device Lett. **33**, 667 (2012).
[14]J. Zhang, X. Kang, X. Wang, S. Huang, C. Chen, K. Wei, Y. Zheng, Q. Zhou, W. Chen, B. Zhang, and X. Liu, IEEE Electron Device Lett. **39**, 847 (2018).
[15]A. Malmros, H. Blanck, and N. Rorsman, Semicond. Sci. Technol. **26**, 075006 (2011).
[16]A. Pooth, J. Bergsten, N. Rorsman, H. Hirshy, R. Perks, P. Tasker, T. Martin, R. Webster, D. Cherns, M. Uren, and M. Kuball, Microelectron. Reliab. **68**, 2 (2017).
[17]Y.-K. Lin, J. Bergsten, H. Leong, A. Malmros, J.-T. Chen, D.-Y. Chen, O. Kordina, H. Zirath, E. Y. Chang, and N. Rorsman, Semicond. Sci. Technol. **33**, 095019 (2018).
[18]A. Calzolaro, R. Hentschel, I. F. Edokam, V. Sizov, T. Mikolajick, and A. Wachowiak, Semicond. Sci. Technol. **35**, 075011 (2020).
[19]M. Spera, G. Greco, R. Lo Nigro, S. Scalese, C. Bongiorno, M. Cannas, F. Giannazzo, and F. Roccaforte, Energies **12**, 2655 (2019).
[20]T. Sato, K. Uryu, J. Okayasu, M. Kimishima, and T. Suzuki, Appl. Phys. Lett. **113**, 063505 (2018).
[21]F. Iucolano, G. Greco, and F. Roccaforte, Appl. Phys. Lett. **103**, 201604 (2013).
[22]H. Berger, Solid State Electron. **15**, 145 (1972).
[23]G. K. Reeves and H. B. Harrison, IEEE Electron Device Lett. **3**, 111 (1982).
[24]H. Kattelus, J. Tandon, and M.-A. Nicolet, Solid State Electron. **29**, 903 (1986).
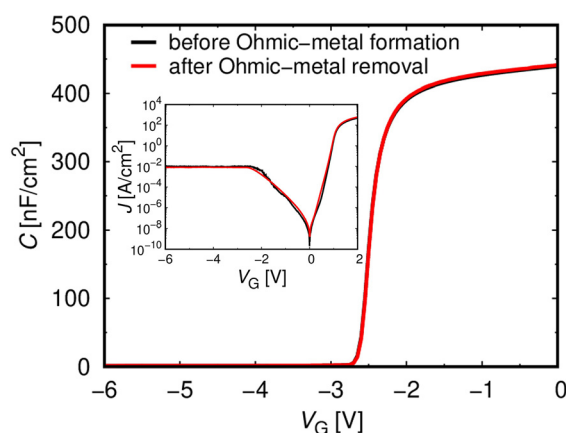[25]H. G. Henry, IEEE Trans. Electron Devices **36**, 1390 (1989).

FIG. 9. The capacitance-voltage characteristics for the Ni/Au Schottky contacts on the AlGaN/GaN heterostructures before Ohmic-metal formation and after Ohmic-metal removal. The inset: the current-voltage characteristics for the Schottky contacts.

[26]M. Ahmad, A. Shah, D. Sharma, N. Roy, and B. Arora, Solid State Electron. **46**, 505 (2002).

[27]M. Hajłasz, J. J. T. M. Donkers, S. J. Sque, S. B. S. Heil, D. J. Gravesteijn, F. J. R. Rietveld, and J. Schmitz, Appl. Phys. Lett. **104**, 242109 (2014).

[28]M. Hajłasz, J. J. T. M. Donkers, S. J. Sque, S. B. S. Heil, D. J. Gravesteijn, F. J. R. Rietveld, and J. Schmitz, in *Proceedings of the 2015 International Conference on Microelectronic Test Structures* (IEEE, 2015), pp. 158–162.

[29]M. Spera, C. Miccoli, R. L. Nigro, C. Bongiorno, D. Corso, S. D. Franco, F. Iucolano, F. Roccaforte, and G. Greco, Mater. Sci. Semicond. Process **78**, 111 (2018).

[30]S. Venica, F. Driussi, A. Gahoi, P. Palestri, M. C. Lemme, and L. Selmi, IEEE Trans. Electron Devices **65**, 1589 (2018).

[31]M. König, G. Ruhl, A. Gahoi, S. Wittmann, T. Preis, J.-M. Batke, I. Costina, and M. C. Lemme, IEEE J. Electron Devices Soc. **7**, 219 (2019).

[32]L. Floyd, T. Scheuermann, P. Herbert, and W. Kelly, Solid State Electron. **37**, 1579 (1994).

[33]D. Sawdai, D. Pavlidis, and D. Cui, IEEE Trans. Electron Devices **46**, 1302 (1999).

[34]M. Lijadi, F. Pardo, N. Bardou, and J.-L. Pelouard, Solid State Electron. **49**, 1655 (2005).

[35]K. Uryu, S. Kiuchi, and T. Suzuki, Appl. Phys. Lett. **119**, 023505 (2021).

[36]I. Halidou, Z. Benzarti, Z. Chine, T. Boufaden, and B. El Jani, Microelectron. J. **32**, 137 (2001).

[37]D. Jena, S. Heikman, D. Green, D. Buttari, R. Coffie, H. Xing, S. Keller, S. DenBaars, J. S. Speck, U. K. Mishra, and I. Smorchkova, Appl. Phys. Lett. **81**, 4395 (2002).

[38]S. Rajan, S. P. DenBaars, U. K. Mishra, H. G. Xing, and D. Jena, Appl. Phys. Lett. **88**, 042103 (2006).

[39]M. Zhu, M. Qi, K. Nomoto, Z. Hu, B. Song, M. Pan, X. Gao, D. Jena, and H. G. Xing, Appl. Phys. Lett. **110**, 182102 (2017).

[40]A. Yu, Solid State Electron. **13**, 239 (1970).

[41]E. L. Murphy and R. H. Good, Phys. Rev. **102**, 1464 (1956).

[42]F. Padovani and R. Stratton, Solid State Electron. **9**, 695 (1966).

[43]K. Osipov, I. Ostermay, M. Bodduluri, F. Brunner, G. Tränkle, and J. Würfl, IEEE Trans. Electron Devices **65**, 3176 (2018).

27 June 2025 03:27:42